CONF-830908--5

UCRL--89771

DE83 017369

# STATUS OF TANDEM-MIRROR CONFINEMENT

D. E. Baldwin and the TMX-U Group

This paper was prepared for submittal to the
11th European Conference on Controlled Fusion
and Plasma Physics, Aachen, Germany,
September 5-9, 1983

August 30, 1983

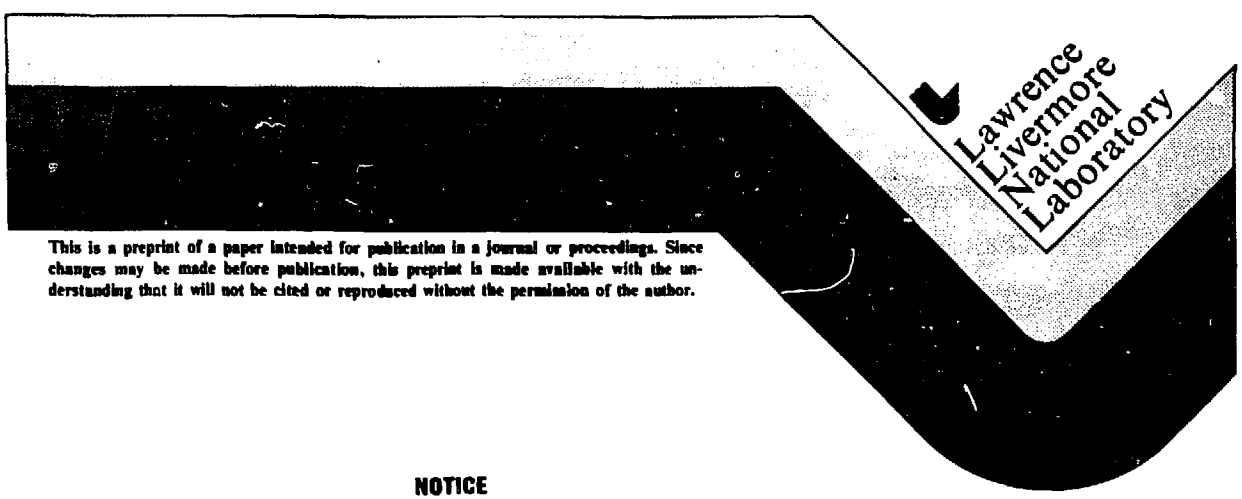

## DISCLAIMER

# STATUS OF TANDEM-MIRROR CONFINEMENT

D. E. Baldwin and the TMX-U Group

Lawrence Livermore National Laboratory
P.O. Box 5511, L-630
Livermore, California 94550 U.S.A.

## ABSTRACT

Recent end-stopping experiments in TMX-Upgrade show strong plugging of the central cell by lower-density plugs, requiring both electron-cyclotron heating (ECRH) and 47° neutral-beam injection, consistent with the thermal-barrier concept. These experiments have low density ($n < 10^{12}$ cm$^{-3}$) due to inefficient ECRH power coupling. Hot-ion and hot-electron buildup are consistent with Fokker-Planck calculations. No ion-cyclotron activity is observed in the plugs; occasional electron-cyclotron activity is observed. With plugging, axial lifetimes ($\tau_{\parallel} > 40$ ms) are larger than radial ($\tau_{\perp} = 5$-10 ms) due to observed non-ambipolar ion transport. Recent tandem-mirror theoretical activities are also surveyed.

## KEYWORDS

Tandem mirrors; end-plugging; thermal barriers.

## INTRODUCTION

The last few months have brought important end-plugging results in the TMX-Upgrade tandem mirror (TM) device. The original TMX was modified during 1980-82 to employ advanced end plugs based on thermal barriers (TB) (Baldwin and Logan, 1979). These TB end plugs use a combination of neutral beam injection and electron cyclotron resonance heating (ECRH) in a way that generates a central cell confining potential $\phi_c$ with plug density $n_p$ less than the central cell density $n_c$. The TMX-U experiment is the first test of TB end plugs.

The recent end plugging experimental results can be summarized as follows:

- Values of $\phi_c = 400$ to 600 eV are routinely generated with $n_c \lesssim 2\, n_p$. Both neutral beams and ECRH are required. There has been no direct measurement of a thermal barrier, but the plasma behavior is consistent with the TB model. With plugging, the axial lifetime $\tau_{\parallel}$ increases by at least one order of magnitude to > 40 ms, not determined.
- Plugging operation to date has been at low density $n_c < 10^{12}$ cm$^{-3}$ to permit ECRH startup; $n\tau$ values are correspondingly low. Higher densities appear to be limited by low ECRH power-coupling efficiency, currently being modified and increased.
- High plasma potential during ECRH is correlated with non-ambipolar ion transport, giving radial lifetimes $\tau_{\perp} = 5$-10 ms that increases with $n_c$.
- No ion cyclotron activity is observed during plugging. Occasional electron cyclotron noise has been observed, thought to be the whistler and upper hybrid loss cone modes, but has not limited buildup or confinement for $\langle\beta\rangle = 3$-5% for hot electrons.

This talk describes some of the support for these conclusions, and reviews some of the important collateral theoretical developments over the past year.

## TMX-U EXPERIMENTAL RESULTS

The magnet and injected power layouts are shown in Fig. 1 (Foote, et. al., 1982). The central cell flux maps to minimum-B end-cells having vacuum mirror ratio $R_m = 4$.

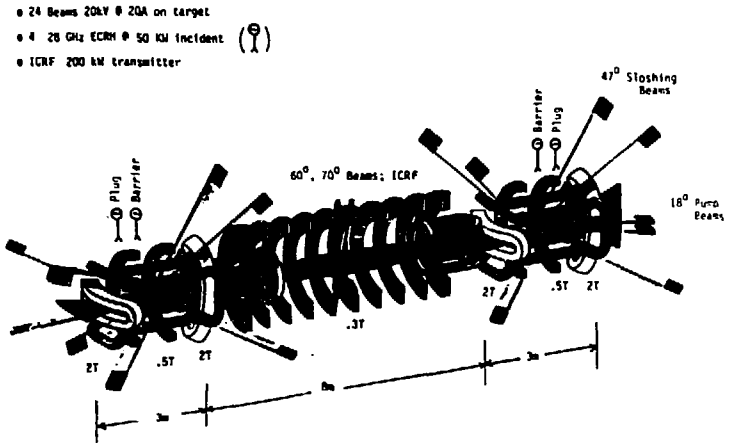


Fig. 1 TMX-Upgrade magnet set and power

Neutral beams for ion heating (~100A on target) are injected into the central cell at 58° and 70° to B. In the end cells the 47°-injected beams (up to 100A on target per plug) create density maxima near their R = 2 turning points, generating a double-lobed, "sloshing ion" density distribution. The density maxima are maintained against ion angle scatter by charge exchange on the 47°-beams and on the 18°-beams (the pump beams) that are injected into the loss cone of the mirror cell.

ECRh at 28 GHz is injected into the plugs at the 5 kG (2nd harmonic) and the outer 10 kG (fundamental) points in narrow beams having single-pass absorption. For the data described, up to 100 kW = 2 X 50 kW per plug for 50 ms has been injected.

ICRF (ion cyclotron heating) is available from a 200 kW transmitter. To date, little plasma heating has been observed due to poor coupling of a 1/4-turn antenna.

The central cell is fueled by controlled gas input through puffer valves and/or an apertured gas box which also acts as a plasma limiter.

The diagnostics used in analyzing the results reported here include diamagnetic loops and microwave interferometers in the central cell and end cells, end loss energy analyzers, Faraday cups, and net current collectors measuring radial loss current profiles to the end walls.

The machine can be operated in both high and low density modes. The high density mode, using relatively high gas inputs with ECRH breakdown, creates a target for neutral beam injection, although it is too high density for ECRH hot-electron build-up with present deliverable ECRH power. The low density mode, using relatively low gas input, permits buildup of hot, anisotropic electrons at densities that trap only a few percent of the injected neutral beam power. This latter mode has been the starting point for the end-plugging experiments, but requires good vacuum conditions for beam buildup.

The high density mode ($n > 10^{12}$ cm$^{-3}$) results have been reported earlier (Simonen, et al., 1983). End plugging is that of a conventional TM in the sense that $n_p > n_c$ and

$\phi_c = T_e \ln(n_p/n_c)$ with $T_e$ the electron temperature. TMX-U differs from TMX due to the sloshing ion distribution which dramatically improves ion cyclotron microstability. In this high density mode in TMX-U, little or no ion cyclotron noise has been observed, and plug-ion profiles and lifetimes are in agreement with classical Fokker-Planck computations. The densities attained in this mode are the TMX-U design values.

An important element for thermal barrier formation is the removal of thermal ions from the potential depression, called "pumping". To some extent the 47°-beams serve this function in TMX-U. The 18°-beams augment the process while not raising the sloshing ion density above ECRH cut-off. Figure 2 demonstrates pumping by charge exchange removal of 47°-ions by the 18° pump beams in high density operation without a potential dip. The figure shows reduction in the total density, diamagnetism, and sloshing ion density with pump beam turn-on, with a 9 ms time constant compared to a 7 ms value calculated for the 54 A's of pump beam current.

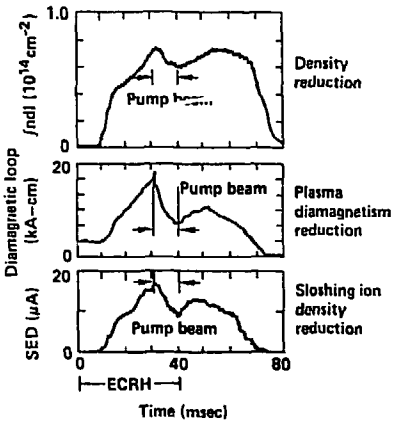


Fig. 2 Demonstration of charge exchange pumping

In the low density mode ($n \leq 10^{12}$ cm$^{-3}$) without neutral injection, the hot electron density in the plug with energy 30-70 keV rises to several times the cold density in the central cell; see Fig. 3 (column 1). The B and density are limited by ECRH power and pulse length. From the rate of rise of diamagnetism, we estimate a 22% coupling efficiency of ECRH to magnetically trapped electrons. Their axial length is ~120 cm and radius is ~13 cm. The 10 kG-resonant heating enhances the electron loss rate from the plug; and, because of the higher plug density, these losses dominate the electron loss. The overall space potential rises to about 1 kV, as measured by an end loss analyser, and the average energy of electron end loss is 0.4 to 1 keV. Ions are confined principally by flow, although there probably is an unmeasured small dip in potential in the plugs, holding the ions that neutralize the hot electrons. The buildup is consistent with Fokker-Planck calculations, although the axial width is somewhat shorter. These conditions form the first stage in the buildup to a plugging configuration, in which the hot-electron density in the plugs has been established.

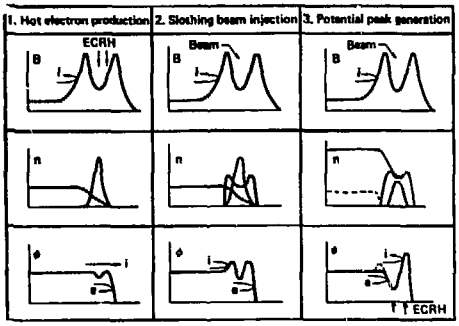


Fig. 3 Thermal barrier startup sequence

Hot ion buildup on this target requires a neutral pressure < $10^{-6}$ Torr which could not be sustained during last winter's operation. A spring shutdown permitted reworking of the vacuum system, to hold $p_0 \approx 0.5 \times 10^{-6}$ Torr throughout the shot. At this pressure the neutral atomic density in the plasma, when reduced by molecular disassociation, is less than the neutral beam atomic density.

The 47°-beams are then injected into the plugs with the intent of charge exchanging the cold ions neutralizing the hot electrons into a sloshing ion density profile that is broader in axial extent than the anisotropic electron profile. This enhances the potential dip at the hot electrons, particularly when the sloshing ion peak density exceeds the central cell density. Then, cold ions cannot flow into the plug to replace those charge exchanged. Theoretically, this potential dip forms a thermal barrier, increasing the isolation of the population of electrons neutralizing the outer lobe of the sloshing-ion distribution beyond that accompanying the density rise. The 10 kG-ECRH can then heat these isolated electrons to an average energy above the central cell temperature. In the experiment the plug potential is observed to rise sharply to 400-600 eV above the central cell, shutting off the central cell ion end loss. With proper gas feed, the central cell density rises to a value as high as twice the plug density. The potential formation is then clearly non-Boltzmann in character. Fig. 3 (column 3) shows qualitative density and potential profiles from modelling of the process in steady state. These details have not been measured directly, but as shown below all the ingredients called for in the model, viz., vacuum, beams, and ECRH, appear to be required in the experiment.

The characteristics of the plugging are shown in Fig. 4. For this data, a plugging potential was built in only one end of the machine (west). Then, the magnitude of the plug-to-central-cell potential difference can be determined from the difference between the minimum energies of ions lost out the two ends, when the residual loss from the plugged end is large enough for a measurement of the minimum energy. Central cell ions are only flow-confined against loss out the east end. When the west ECRH power is turned on, the diamagnetism builds up, and the densities come to steady state (here $n_c \approx 4\ n_p$) with loss out both ends having equal minimum energies. With the turn-on of the beam current, the west end loss drops abruptly and stays small until the ECRH is turned off. The measured end loss at this time implies a lifetime against axial loss of 40 ms, but energetic electrons and ionization in the end tank make small unknown contributions to the measured current. (The simultaneous rise of $n_c$ and end loss on ECRH turnoff are discussed later.)

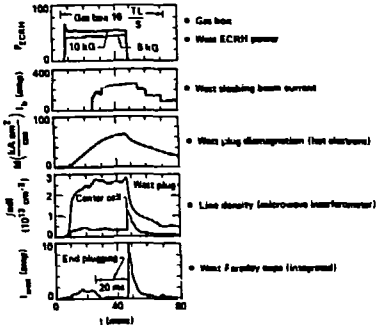


Fig. 4 Demonstration of ECRH end plugging

The necessity for the sloshing beams is demonstrated by a shot having brief beam-current interrupts as shown in the top trace of Fig. 5. The end loss shows corresponding brief increases with measureable response times. The recoverability suggests the robustness of the configuration; the 0.3 ms rise time and 2 ms decay time for plugging are consistent with classical build-up and decay of sloshing ions.

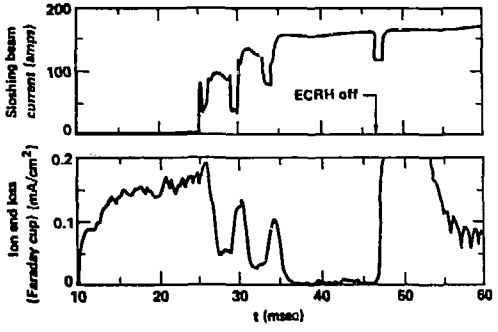


Fig. 5 Demonstration of required sloshing-ion beams

The different roles played by the two ECRH frequencies is shown in Fig. 6, where are shown the results of early turn-off of each. The barrier ECRH (5 kG) forms a hot ($\sim$ 50 keV) mirror-confined population which lives long after its ECRH turn off (see the diamagnetism trace in Fig. 4). Potential formation is, therefore, not affected by early turnoff of this power (provided it had been on initially!). The end plugging ECRH (10 kG) heats the electrons isolated in the plugging potential to an average energy $\approx$1 keV. Early turn-off of this power leads to a loss of plugging potential on the time scale of electron scatter at their average energy and the total density ($\approx$3 ms). This difference in behavior is completely consistent with the TB models.

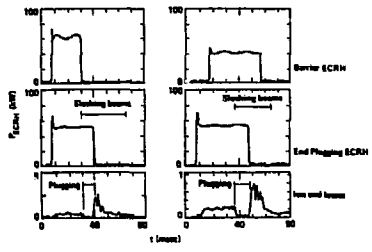

Fig. 6 Demonstration of required ECRH

A sample shot plugging both ends is shown in Fig. 7. The trace shows the time history of the indicated quantities for the east end, central cell, and west end over the 80 ms. shot. The insert shows the timing of gas sources. The ECRH and beam power are similar to Fig. 4. The east diamagnetism loop saturates due to the lower 10 kG ECRH power. End-cell neutral-beam turn on at 35 ms initiates plugging and central cell density buildup. This data was taken while we were learning how to increase the central cell density with gas feed, consequently the density history is quite irregular. Here, $n_c \approx n_p$ (west) with allowance for different plasma radii ($r_c \approx 1.3\ r_p$). The highest values observed on other shots have $n_c \approx 2\ n_p$.

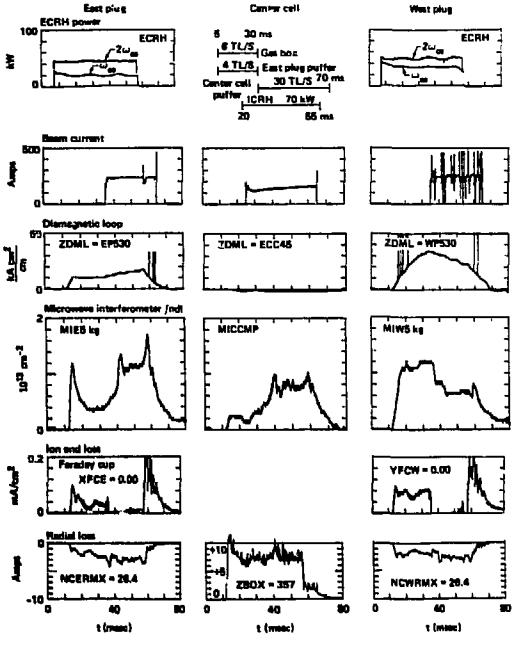


Fig. 7 Double-ended plugging

The sharp rise in end loss current, without an associated drop in central cell density, sugggests the seccession of another loss process. This process is a non-ambipolar ion transport correlated with the 10 kG ECRH, probably associated with the high plasma potentials. It is present with or without plugging. It is evidenced by the net electron current measured at the end wall. The integrated value out to a central-cell radius of 26 cm. is shown in Fig. 7. At the same time there is a net ion current to the gas box. Both drop with the 10 kG ECRH power. The 5A drop to the gas box clearly accounts for the sum of the decreases on the two integrated net current detectors. Both are independent of central cell density, during the buildup as shown here and in other shots having twice the central cell density.

During the occurence of this transport, no coherent r.f. activity is observed in the device, e.g., as might indicate a coherent, low-m rotation-driven instability. There is always present a turbulent spectrum ($\phi^2 \propto \omega^{-1}$) whose amplitude is higher during conditions of transport. A turbulence-driven transport in the central cell would presumably be ambipolar. This would not be measured by the net current analyzers. As estimated, by particle accountibility, this transport could be as high as several times the non-ambipolar transport. We are continuing to treat turbulence as a candidate for transport, e.g., in the plugs where hot electrons would not be transported, as well as evaluating known causes for non-ambipolar mechanisms, such as neo-classical and resonation transport and charge-exchange-induced mobility.

An important feature of TMX-U operation during plugging is the total absence of ion cyclotron activity in the plugs. This was predicted by theory as an important adjunct of hot and warm plasma density profiles occuring in a TB end plug. Briefly, as seen from the $\phi$-profile in Fig. 3 (column 3), warm ions penetrate to the plug midplane, rendering the distribution there monotonic in energy. The observed stability further supports the evidence for a TB profile in TMX-U. As the plug density is increased and $c/\omega_{pi}$ decreases, modes become increasingly able to localize in the outer peak potential where the energy distribution is not monotone. However, TMX-U is calculated to remain stable at its designed higher-density operating point. The observed stability during the high density operation without hot electrons supports this.

Electron cyclotron activity above thermal level is occasionally observed in TMX-U, either below $\omega_{ce}$ taken to be the whistler mode or at $\omega_{ce}$ taken to be the upper-hybrid loss-cone (UHLC) mode, both of which are predicted to be convectively unstable. (Casper, et al., 1983). In some cases this limits the density and/or the energy buildup; in other cases buildup is limited only by ECRH power and duration. Figure 8 shows the theoretical convective growth length curves for both modes for the density ratio $n_{eh}/n = 0.6$ having the shortest UHLC growth length. As can be seen, while we have not yet encountered any basic limitation by hot electron instabilities, shorter convective growth lengths are predicted as the density increases.

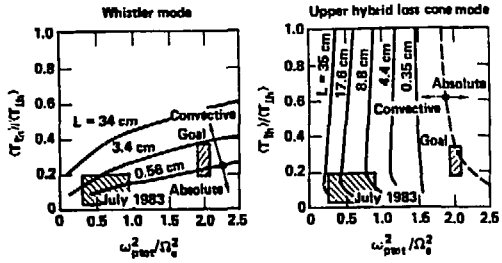


Fig. 8 Electron microstability analysis

Several modifications are currently being installed in TMX-U which are designed to extend the recent endplugging results to higher densities. The are predicated on the interpretation that the observed density limits have been due to limits in power to the plasma. An ECRH quasi-optical waveguide will replace the past multi-arm waveguide and a double 1/2-turn ICRF antenna will replace the past 1/4-turn antenna. Because of the observed correlation between high plasma potential and transport, we are also embarking on experiments designed to control the radial potential profile by shaping the end-wall potential profile on a segmented end wall.

## OTHER TANDEM MIRROR FACILITIES

The PHAEDRUS TM has operated at the University of Wisconsin for several years, focusing on the applications of ICRF to TM operation. Recent results include generation of sloshing-ion distributions and MHD stabilization of an axisymmetric geometry using ICRF. The latter is thought to arise from the effect of radial gradients of pondromotive potential on particle drifts. PHAEDRUS has also demonstrated variation of the radial electric field within the plasma by controlling the bias on segmented end walls.

Three important TM devices are nearing completion, the GAMMA 10 at Tsukuba, Japan, and TARA at MIT, and the AMBAL at Novosibirsk, USSR. GAMMA-10 and TARA will explore variations in magnetic geometry, with particular emphasis on more nearly axisymmetric approaches. AMBAL will focus on the basic physics of equilibrium, stability and transport in hot, tandem mirror plasmas.

## HIGHLIGHTS OF TANDEM MIRROR THEORY

Much of tandem-mirror theory effort can be grouped into three areas:

( i) Synthesis and integration of physics output from specialized studies into the physics design of experimental facilities and into the development of global performance-simulation and optimization rate codes.

( ii) Detailed numerical evaluation of fundamental processes in realistic geometry in 1,2, and (sometimes) 3 velocity and/or configuration-space dimensions.

(iii) Studies of basic processes, often analytic, in idealized geometry.

The past couple of years have brought important advances in all three areas.

The results of equilibrium and transport theory, described below, have been applied to the magnet designs of MFTF-B, Gamma 10, and TARA. These have focussed on the role played by the geodesic component of magnetic line curvature and have evolved designs having its average vanish, thereby minimizing transport and distortion of the central cell by parallel currents. These results have been optimized in a TM reactor conceptual design MARS (Mirror Advance Reactor Study) with a volume-averaged $\langle\beta\rangle = 30\%$ limit against the worst (m = 1) MHD-balloon mode (Logan, et al., 1982).

The advent of thermal barriers increases the role of non-Maxwellian distributions in TM's, including the coupling between cells by particles of low collisionality. Development by Matsuda and Stewart (1983) of a finite-element, bounce-averaged, multi-region Fokker-Planck code including r.f. interaction has greatly increased our descriptive capability. This code is currently being applied to problems of ECRH buildup and maintenance, plug-electron heating and potential formation, and thermal barrier passing-ion trapping and pumping.

Tandem mirrors are subject to a special form of ion transport arising from a resonance between azimuthal-drift and axial-bounce frequencies (Ryutov and Stupakov 1977, 1978a, 1978b). These effects have been contained in a transport code that also contains axial end loss and various atomic physics packages (Mirin, et al., 1983). As well as modelling a variety of experimental conditions, the code has been used to evaluate radial electric field control by means of a profiled biasing of end-wall potentials.

Tandem mirror MHD-equilibria are fully 3-dimensional, made simpler by being paraxial in character. Solutions to date include a $\beta$-expansion (Pearlstein, et al., 1981) and a rigid profile (Pearlstein, 1983). A reduced MHD description reported earlier (Bulmer, et al., 1983) describes general $\beta$ and profiles. These equilibrium codes are routinely run by magnet designers, and the results have strongly influenced both conceptual and detailed aspects of the designs mentioned above.

In TB modelling an important determination is the magnitude of plugging potential outside the thermal barrier. Early modelling treated the plug-potential-trapped electrons as quasi-Maxwellian with elevated temperature, leading to a logarithmic dependence of potential as density. Analytic (Cohen, 1983) and Fokker-Planck/Monte-Carlo simulations (Matsuda and Rognlien, 1983) finds the trapped electron distribution to be flattened in energy, giving a more favorable relationship, approximately

$$\phi_c = T_{ec} \left\{ \left[ \frac{n_p}{2n_c} \left( \frac{n_c}{n_b^*} \right)^{4/3} \right]^{2/3} - \ln \frac{n_c}{n_b^*} \right\}$$

where $T_{ec}$ is the central cell electron temperature and $n_b^*$ is the thermal electron density at the barrier. This result relaxes the required hot electron density fraction at the barrier $n_{eh} = n_{ion,b} - n_b^*$.

Over the years, much of mirror theory has been devoted to the ion-cyclotron fluctuations so prominent in mirror devices. This theory predicted stable conditions with sloshing-ion thermal barriers, and the early results from TMX-U are most encouraging. If this problem indeed proves to be a thing of the past, these results will constitute a real milestone.

The most recent important stability results deal with the possibility of rapidly growing electrostatic trapped-particle modes, driven by particles trapped in unfavorable curvature regions (Berk, et al., 1983). Theoretically, stability to these modes sets a minimum on the fraction of particles that must link good and bad curvature regions. Very preliminary experiments in TMX observed a low frequency oscillation, not affecting confinement, when this calculated fraction was not satisfied. Because the conditions for stability set by this mode have a large leverage on projected reactor performance, future experiments delineating these conditions will be closely watched.

## MFTF-B STATUS

MFTF-B is the large tandem mirror facility under construction at Livermore, currently due for operation in 1986, that is designed to approach scientific breakeven. It brings together all of the elements contained in the MARS conceptual reactor. In mid-1982 the magnetic geometry was converted to an axicell geometry, having a high-field coil (or possibly an axisymmetric mirror cell) inserted at the ends of the central cell, before the transition region, see Fig. 9.

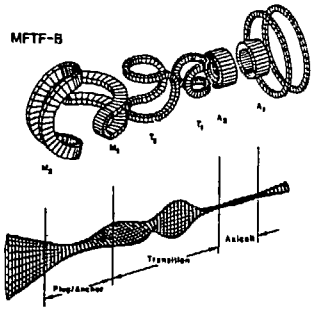


Fig. 9 The MFTF-B end-cell magnet set

These mirrors confine much of the central cell ions magnetically and reduce the density in the plugs for more efficient plug potential creation. The axicell design generates the highest magnetic fields by circular coils.

The transition to the plug is of a "double-fan" type, having two fan-shaped regions of opposite-signed geodesic curvature. The designed zero-average of geodesic curvature minimizes transport step size and the generation of parallel (Pfirsch-Schluter) current in the central cell.

## SUMMARY

The thermal barrier mode of operating a tandem mirror appeared to offer such improvements that several new devices were designed to incorporate TB's solely on the basis of their theoretical value. The first TB results from TMX-U lend confidence that our thinking was well founded, at least qualitatively. However, much remains to be done in verifying and quantifying our theoretical modelling.

## ACKNOWLEDGEMENT

We are grateful to Dana Richards for preparation of this manuscript. This work was performed under the auspices of the U.S. Department of Energy by the Lawrence Livermore Laboratory under Contract W-7405-Eng-48.

## REFERENCES

Baldwin, D.E. and B.G. Logan, (1979) Phys Rev. Lett. 43, 1318
Berk, H.L., M.N. Rosenbluth, H.V. Wong, T.M. Antonsen, D.E. Baldwin, and B. Lane, 9th Int. Conf. on Plasma Phys. and Cont. Fus. Res., Baltimore (1982), IAEA CN-41/K-3.
Bulmer, R.H., T.B. Kaiser, W.M. Nevins, W.A. Newcomb, L.D. Pearlstein, H.R. Strauss, S. Wollman, and M. Wakatani (1983), 9th Conf. on Plasma Phys. and Cont. Fus. Res., Baltimore (1982) IAEA Vol. 1, 531.
Casper, T.A., Y.-J. Chen, R. Ellis, R. James, C. Lasnier (1983), Assessment of Hot Electron Microstability in the Initial TMU Experiments, Livermore UCID-19783.
Cohen, R.H. (1983), to appear in Phys. Fluids Letts. October.
Foote, J.H., A.K. Chargin, R.H. Cohen, T.B. Kaiser, C.V. Karmandy, T.C. Simonen, and R.L. Wong (1982) J. of Fusion Eng. 2, 383.
Logan, B.G., et al., Mirror Advanced Reactor Study Interim Design Report, LLNL UCRL-53333 (1983); a final report is due this fall.
Matsuda, Y. and J.J. Stewart, (1983), "Solution of Bounce-Averaged Fokker-Planck Equation for a Multi-Valued Distribution Function by a Finite Element Method-Abstract," 10th Conference on Numerical Simulation of Plasmas, San Diego, CA., LLNL UCRL-88364.
Matsuda, Y., and T. Rognlien (1983), to appear in Phys. Fluids Letts, October.
Mirin, A.A., S.P. Auerbach, R.H. Cohen, J.M. Gilmore, L.D. Pearlstein, M.E. Rensink, (1983) Nucl. Fus. 23, 703.
Pearlstein, L.D., T.B. Kaiser, W.A. Newcomb (1981) Phys. Fluids 24, 1326.
Pearlstein, L.D. (1983) Int. Sch. of Plasma Phys., Varenna, Sept. 7-17, LLNL UCRL - 89767.
Ryutov, D.D., G.V. Stupakov, (1977) Pisma Zhk. Eksp. Thes. F.7 26, 186; (1978a) Dokl. Akad. Nauk. SSSR 240, 1086; (1978b) Fiz. Plasmy 4, 501.
Simonen, T.C., et al. (1983) Phys. Rev. Letts 50, 1668.